PAPER

Pattern Synthesis of Spatial Eigenmodes Exploiting Spherical Conformal Array

Akira SAITOU[†a)], **Ryo ISHIKAWA**[†], ***Members***, ***and*** **Kazuhiko HONJO**[†], ***Fellow***

SUMMARY Unique spatial eigenmodes for the spherical coordinate system are shown to be successfully synthesized by properly allocated combinations of current distributions along θ' and ϕ' on a spherical conformal array. The allocation ratios are analytically found in a closed form with a matrix that relates the expansion coefficients of the current to its radiated field. The coefficients are obtained by general Fourier expansion of the current and the mode expansion of the field, respectively. The validity of the obtained formulas is numerically confirmed, and important effects of the sphere radius and the degrees of the currents on the radiated fields are numerically explained. The formulas are used to design six current distributions that synthesize six unique eigenmodes. The accuracy of the synthesized fields is quantitatively investigated, and the accuracy is shown to be remarkably improved by more than 27 dB with two additional kinds of current distributions.

key words: *pattern synthesis, eigenmode, spherical conformal array, numerical calculation*

1. Introduction

The spatial eigenmode has been attracting interest both for analytical and practical applications for antennas. It has been utilized to analyze input impedances and radiation patterns of various antennas and arrays [1]–[9]. One of the most important features is the orthogonality among the eigenmodes, and the complexity of the analysis has been remarkably reduced due to that feature.

The orthogonality is also exploited for practical applications, such as spatial multiplexing for high-speed Multi-Input Multi-Output (MIMO) communication and more detailed information for sensing. As for the sensing of the direction of arrival, both the scalar sonic eigenmodes and the vector electromagnetic eigenmodes are exploited [10], [11]. On the other hand, Orbital Angular Momentum (OAM) communication has recently been attracting attention for line-of-sight communication, where orthogonal vector OAM eigenmodes with different angular momenta are exploited to realize independent communication channels [12]–[20]. A feature of the OAM eigenmode is its spatial distribution of $\exp(jm\phi)$ in the spherical coordinate system, where m denotes the index that is called the phase mode number or the magnetic quantum number. When different signal sequences are overlaid on n kinds of OAM eigenmodes with different $m\hbar$ OAMs, n-channel multiplexing communication becomes possible due to the orthogonality.

To extend the communication distance, higher gain has been pursued, and horn antennas have been used to increase the element gain. On the other hand, a communication scheme with paraboloids has been proposed by the authors [18]–[20], where the far fields of the OAM eigenmodes radiated by the loop antenna array are collimated by the paraboloids. According to the geometric optics, electromagnetic field distribution around the receiving area is considered to be almost identical to that around the transmitting area except the sign of the wave number vector. The current distributions are also almost identical except their directions. In this case, where the current distribution at the transmitting array is adjusted to radiate a unique mode, the receiver consisting of the same array receives only the unique mode. Thus, the current distribution at the receiver becomes almost identical to that at the transmitter. This behavior has been confirmed by simulations and measurements.

However, there are many more independent eigenmodes in free space, because each eigenmode is defined by the OAM quantum number l as well as the magnetic quantum number m for each Transverse Electric (TE) and Transverse Magnetic (TM) wave. Thus, if the eigenmodes are fully utilized, many more independent channels would be available. Thus, optimal design method of MIMO antenna directivities and corresponding current distributions has been analyzed [21]. However, to extend the communication distance, synthesizing unique modes with respect to both l and m for each TE and TM wave is anticipated for the communication scheme with the paraboloids. For the purpose of the synthesis, two-dimensional current distribution would be required, possibly because the OAM mode radiated by the one-dimensional circular current is unique only for m but degenerate with regard to l [18]. To synthesize fully unique modes, the spherical conformal array is a viable candidate as it offers two-dimensional currents and consistency with spherical coordinates. It is obvious that many kinds of practical and essential problems should be simultaneously addressed such as mutual impedance effects [22]–[24] and design of element layout and assembly [25]–[29]. Whereas the effects are neglected in this paper, the current for the unique mode is also indispensable, because it is the targeted current after compensating for the effects.

In Sect. 2 of this paper, the current distribution for the unique mode is analytically obtained by neglecting the mutual impedance effect. With the matrix that relates the cur-

Manuscript received October 27, 2021.
Manuscript revised February 9, 2022.
Manuscript publicized April 6, 2022.

[†]The authors are with the University of Electro-Communications, Chofu-shi, 182-8585 Japan.
a) E-mail: asaitou@uec.ac.jp

DOI: 10.1587/transcom.2021EBP3175

rents to the fields, the current for the unique mode is analytically found. To estimate the validity, the numerically calculated results are shown in Sect. 3. After confirming the consistency of the obtained formulas, important features of the matrix elements are clarified. From the results, the current distributions for the unique modes are numerically found. In addition, the accuracy of the synthesized fields is investigated and remedial measures are provided.

2. Analytical Expression for Relation of the Current and Electric far Field with Matrices

Where some current distribution is given, its radiated electromagnetic field is analytically found with the vector potential. However, it is usually difficult to find the current distribution that yields some desired field. Here, to obtain the far field of the unique mode, discreet coefficients for both the current on the spherical array and radiated fields are derived with the general Fourier expansion and the mode expansion, respectively. The relation of the coefficients is described with a matrix, and the combinations of the currents for the unique modes are found in closed form with the inverse matrix.

2.1 Discreet Expression of Current on Spherical Array

Figure 1 shows the analyzed configuration of the current density on the spherical array. Each current source is assumed to be realized by continuous infinitesimal elements and its input impedance is assumed to be impedance-matched to the port impedance R_0. P is an observation point to estimate the radiated field. To discreetly express the currents flowing along θ' and ϕ' on a spherical array, their distributions are general Fourier–expanded with the spherical harmonics as follows, where a and $P_n^m(\mathrm{x})$ denote the radius of the sphere and the associated Legendre function for the degree of n and the order of m [30], respectively:

$$J_{\theta'} = \sum_{n=0}^{\infty}\sum_{m=-n}^{n}\left\{c\theta_{nm}\sqrt{\frac{(n-m)!(2n+1)}{2\cdot(n+m)!}}P_n^m(\cos\theta')e^{jm\phi'}\right\}\delta(r-a) \tag{1}$$

$$J_{\phi'} = \sum_{n=0}^{\infty}\sum_{m=-n}^{n}\left\{c\phi_{nm}\sqrt{\frac{(n-m)!(2n+1)}{2\cdot(n+m)!}}P_n^m(\cos\theta')e^{jm\phi'}\right\}\delta(r-a). \tag{2}$$

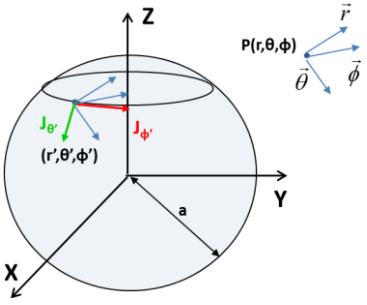

Fig. 1 Configuration of analyzed current density.

As the mutual impedances are neglected, the input power for $J_{\theta'}$ can be estimated as follows:

$$P_{in}(n,m) = \frac{a^2}{2}\iint\left\{R_0|J_{\theta'}|^2\right\}\sin\theta' d\theta' d\phi' = \pi a^2 R_0|c\theta_{nm}|^2. \tag{3}$$

The input power is independent of n and m, and is proportional to $|c\theta_{n,m}|^2$. Similarly, the input power is proportional to $|c\phi_{n,m}|^2$.

2.2 Discreet Expression of Radiated Fields

In the far-field region, the electric field is given with the vector potential by (4) [31], where the assumed time convention is $\exp(-j\omega t)$.

$$\mathbf{E} = j\omega\begin{bmatrix}0\\A_\theta\\A_\phi\end{bmatrix}. \tag{4}$$

The far-field vector potential is found with the current distribution, as follows:

$$\begin{bmatrix}A_\theta\\A_\phi\end{bmatrix} = \frac{\mu_0}{4\pi}\frac{e^{jkr}}{r}\iiint_V\begin{bmatrix}J_\theta\\J_\phi\end{bmatrix}e^{-jka\{\sin\theta\sin\theta'\cos(\phi'-\phi)+\cos\theta\cos\theta'\}} r'^2\sin\theta' dr' d\theta' d\phi'. \tag{5}$$

To obtain the vector potential elements for θ and ϕ, the current density J_θ and J_ϕ is expressed with the coordinate transformation formula as follows, where $J_{\theta'}$ and $J_{\phi'}$ are defined by (1) and (2):

$$\begin{bmatrix}J_\theta\\J_\phi\end{bmatrix} = \begin{bmatrix}\{\cos\theta'\cos(\phi'-\phi)\cos\theta+\sin\theta'\sin\theta\}J_{\theta'}-\cos\theta\sin(\phi'-\phi)J_{\phi'}\\ \cos\theta'\sin(\phi'-\phi)J_{\theta'}+\cos(\phi'-\phi)J_{\phi'}\end{bmatrix}. \tag{6}$$

Thus, the electric far fields radiated by the currents are found with (4), (5) and (6).

Integration for θ' and ϕ' can be carried out with the formulas of (7) and (8), and the electric field is found as shown in (9) and (10), where $\mathbf{E}^{c\theta_{nm}}$ and $\mathbf{E}^{c\phi_{nm}}$ are electric fields radiated by $(n,m)^{\text{th}}$ $J_{\theta'}$ and $J_{\phi'}$, respectively.

$$J_m(x) = \frac{1}{2\pi}\int_0^{2\pi}\exp[j(m\phi' - x\sin\phi')]d\phi' \tag{7}$$

$$J_m(ka\sin\theta\sin\theta')\exp(-jka\cos\theta\cos\theta') = \sum_{l=0}^{\infty}(-j)^{l+m}(2l+1)j_l(ka)P_l^{-m}(\cos\theta)P_l^m(\cos\theta'). \tag{8}$$

To express the relation between the current and the electric field with a matrix, the obtained fields were mode-expanded with the spatial eigenmodes in the far field. For the far fields, the electric field $\boldsymbol{E}$ and the magnetic field $\boldsymbol{H}$ are uniquely related as shown in (12), and the electromagnetic fields can be described only with the electric field.

$$\mathbf{E}^{c\theta_{nm}} = \alpha a(n,m)\frac{e^{jkr}}{kr}c\theta_{nm}(-1)^m e^{jm\phi}\sum_{l=0}^{\infty}(-j)^l\frac{(2l+1)}{2}j_l(ka)$$
$$\times\left[\begin{array}{c} 2\sin\theta P_l^{-m}(\cos\theta)\displaystyle\int_{-1}^{1}\sqrt{1-x^2}P_n^m(x)P_l^m(x)dx - P_l^{-m+1}(\cos\theta)\cos\theta\int_{-1}^{1}xP_n^m(x)P_l^{m-1}(x)dx - P_l^{-m-1}(\cos\theta)\cos\theta\displaystyle\int_{-1}^{1}xP_n^m(x)P_l^{m+1}(x)dx \\ -\dfrac{2m}{ka\sin\theta}P_l^{-m}(\cos\theta)\displaystyle\int_{-1}^{1}\frac{x}{\sqrt{1-x^2}}P_n^m(x)P_l^m(x)dx \end{array}\right] \tag{9}$$

$$\mathbf{E}^{c\phi_{nm}} = \alpha a(n,m)\frac{e^{jkr}}{kr}c\phi_{nm}(-1)^m e^{jm\phi}\sum_{l=0}^{\infty}(-j)^l\frac{(2l+1)}{2}j_l(ka)\left[\begin{array}{c} \dfrac{2m\cot\theta}{ka}P_l^{-m}(\cos\theta)\displaystyle\int_{-1}^{1}\frac{1}{\sqrt{1-x^2}}P_n^m(x)P_l^m(x)dx \\ -P_l^{-m+1}(\cos\theta)\displaystyle\int_{-1}^{1}P_n^m(x)P_l^{m-1}(x)dx - P_l^{-m-1}(\cos\theta)\displaystyle\int_{-1}^{1}P_n^m(x)P_l^{m+1}(x)dx \end{array}\right] \tag{10}$$

$$\alpha = \frac{j(ka)^2\eta}{2} \quad a(n,m) = \sqrt{\frac{(n-m)!(2n+1)}{2\cdot(n+m)!}}. \tag{11}$$

$$E_r = H_r = 0, \quad E_\theta = \eta H_\phi, \quad E_\phi = -\eta H_\theta. \tag{12}$$

Accordingly, the orthogonal relation in the far field is also described only with the electric fields, as shown in (13). R is the radius of the sphere for the integration, and this sphere encloses the spherical array.

$$\int_0^{2\pi}\left\{\int_0^{\pi}\left\{\frac{1}{2}\mathrm{Re}\left[\mathbf{E}_1\times\mathbf{H}_2^*\right]\right\}_r R^2\sin\theta d\theta\right\}d\phi = \frac{1}{2\eta}\int_0^{2\pi}\left\{\int_0^{\pi}\left(\mathbf{E}_1\cdot\mathbf{E}_2^*\right)R^2\sin\theta d\theta\right\}d\phi = 0. \tag{13}$$

The eigenmodes can also be described with only the electric field, as shown in (14) and (15).

$$\mathbf{E}_{l'm'}^{TM} = b(l',m')\frac{1}{r}e^{jkr}e^{jm'\varphi}\left[\begin{array}{c} 0 \\ -\dfrac{\partial P_{l'}^{m'}(\cos\theta)}{\partial\theta} \\ -j\dfrac{m'}{\sin\theta}P_{l'}^{m'}(\cos\theta)\end{array}\right]. \tag{14}$$

$$\mathbf{E}_{l'm'}^{TE} = b(l',m')\frac{1}{r}e^{jkr}e^{jm'\varphi}\left[\begin{array}{c} 0 \\ \dfrac{jm'}{\sin\theta}P_{l'}^{m'}(\cos\theta) \\ -\dfrac{\partial P_{l'}^{m'}(\cos\theta)}{\partial\theta}\end{array}\right] \tag{15}$$

$$b(l',m') = (-j)^{l'}\sqrt{\frac{(2l'+1)\eta}{2\pi l'(l'+1)}\frac{(l'-m')!}{(l'+m')!}} \tag{16}$$

$$\frac{1}{2\eta}\int_0^{2\pi}d\varphi\int_0^{\pi}|\mathbf{E}_{l'm'}^{TM}|^2R^2\sin\theta d\theta = \frac{1}{2\eta}\int_0^{2\pi}d\varphi\int_0^{\pi}|\mathbf{E}_{l'm'}^{TE}|^2R^2\sin\theta d\theta = 1. \tag{17}$$

$\mathbf{E}_{l'm'}^{TM}$ and $\mathbf{E}_{l'm'}^{TE}$ denote TM- and TE-wave eigenmodes for the degree of l' and the order of m', respectively. The eigenmodes are orthogonal to each other and are normalized as shown in (17). Thus, the radiated power for each eigenmode is identically normalized irrespective of l' and m'.

As the eigenmodes are complete, the electric fields shown in (9) and (10) can also be uniquely expanded with the eigenmodes as shown in (18) and (19), where ξ and ζ denote the expansion coefficients for TM- and TE-wave eigenmodes, respectively:

$$\mathbf{E}^{c\theta_{nm}} = c\theta_{nm}\sum_{l'=1}^{\infty}\sum_{m'=-l'}^{l'}\left(\xi_{l'm'}^{c\theta_{nm}}\mathbf{E}_{l'm'}^{TM} + \zeta_{l'm'}^{c\theta_{nm}}\mathbf{E}_{l'm'}^{TE}\right) \tag{25}$$

$$\mathbf{E}^{c\phi_{nm}} = c\phi_{nm}\sum_{l'=1}^{\infty}\sum_{m'=-l'}^{l'}\left(\xi_{l'm'}^{c\phi_{nm}}\mathbf{E}_{l'm'}^{TM} + \zeta_{l'm'}^{c\phi_{nm}}\mathbf{E}_{l'm'}^{TE}\right). \tag{26}$$

The expansion coefficients are found as follows, due to the orthogonality:

$$\left.\begin{aligned}\xi_{l'm'}^{c\phi_{nm}} &= \frac{1}{2\eta c\phi_n^m}\int_0^{2\pi}d\phi\int_0^{\pi}(\mathbf{E}^{c\phi_n^m},\mathbf{E}_{l'm'}^{TM})r^2\sin\theta d\theta \\ \zeta_{l'm'}^{c\phi_{nm}} &= \frac{1}{2\eta c\phi_n^m}\int_0^{2\pi}d\phi\int_0^{\pi}(\mathbf{E}^{c\phi_n^m},\mathbf{E}_{l'm'}^{TE})r^2\sin\theta d\theta \\ \xi_{l'm'}^{c\theta_{nm}} &= \frac{1}{2\eta c\theta_{nm}}\int_0^{2\pi}d\phi\int_0^{\pi}(\mathbf{E}^{c\theta_n^m},\mathbf{E}_{l'm'}^{TM})r^2\sin\theta d\theta \\ \zeta_{l'm'}^{c\theta_{nm}} &= \frac{1}{2\eta c\theta_{nm}}\int_0^{2\pi}d\phi\int_0^{\pi}(\mathbf{E}^{c\theta_n^m},\mathbf{E}_{l'm'}^{TE})r^2\sin\theta d\theta.\end{aligned}\right\} \tag{20}$$

After lengthy but simple calculations, the expansion coefficients are found as shown in (21)–(24).

As the formulas are complex, important features of the coefficients are listed below. As all the coefficients include the Kronecker delta ($\delta_{m,m'}$), m for the current and m' for the electric field are identical. On the other hand, even where n for the current is unique, there exist radiated fields for infinite kinds of l'.

The $\xi_{l'm'}^{c\phi_{nm}}$ and $\zeta_{l'm'}^{c\theta_{nm}}$ are proportional to m. In the case where m is zero, the TM wave is not radiated from the current along ϕ', and the TE wave is not radiated from the current along θ'. In other words, the current along θ' radiates only TM waves, and the current along ϕ' radiates only TE waves.

The relation for the parity between n and l' is limited, as shown in Table 1. This relation can be derived by con-

$$\xi^{c\phi_{nm}}_{l'm'} = \frac{\pi m\delta_{m,m'}}{k\eta}\alpha a(n,m)b(l',m)(-1)^m\sum_{l=0}^{\infty}(-j)^{l-l'}\frac{(2l+1)}{2}j_l(ka)\left\{\frac{2}{ka}\int_{-1}^{1}xP_l^{-m}(x)\frac{\partial P^m_{l'}(x)}{\partial x}dx\cdot\int_{-1}^{1}\frac{1}{\sqrt{1-x^2}}P^m_n(x)P^m_l(x)dx\right.$$
$$\left.-j\int_0^{\pi}\frac{1}{\sqrt{1-x^2}}P^m_{l'}(x)P_l^{-m+1}(x)dx\cdot\int_{-1}^{1}P^m_n(x)P^{m-1}_l(x)dx-j\int_{-1}^{1}\frac{1}{\sqrt{1-x^2}}P^m_{l'}(x)P_l^{-m-1}(x)dx\cdot\int_{-1}^{1}P^m_n(x)P^{m+1}_l(x)dx)\right\} \quad (21)$$

$$\xi^{c\phi_{nm}}_{l'm'} = \frac{\pi m\delta_{m,m'}}{k\eta}\alpha a(n,m)b(l',m)(-1)^m\sum_{l=0}^{\infty}(-j)^{l-l'}\frac{(2l+1)}{2}j_l(ka)\left\{\frac{2jm^2}{ka}\int_{-1}^{1}\frac{x}{1-x^2}P^m_{l'}(x)P^{-m}_l(x)dx\cdot\int_{-1}^{1}\frac{1}{\sqrt{1-x^2}}P^m_n(x)P^m_l(x)dx\right.$$
$$\left.+\int_{-1}^{1}\sqrt{1-x^2}P_l^{-m+1}(x)\frac{\partial P^m_{l'}(x)}{\partial x}dx\cdot\int_{-1}^{1}P^m_n(x)P^{m-1}_l(x)dx+\int_{-1}^{1}\sqrt{1-x^2}P_l^{-m-1}(x)\frac{\partial P^m_{l'}(x)}{\partial x}dx\cdot\int_{-1}^{1}P^m_n(x)P^{m+1}_l(x)dx\right\} \quad (22)$$

$$\xi^{c\theta_{nm}}_{l'm'} = \frac{\pi\delta_{m,m'}}{k\eta}\alpha a(n,m)b(l',m)(-1)^m\sum_{l=0}^{\infty}(-j)^{l-l'}\frac{(2l+1)}{2}j_l(ka)\left[-\frac{2jm^2}{ka}\int_{-1}^{1}\frac{1}{1-x^2}P^m_{l'}(x)P^{-m}_l(x)dx\cdot\int_{-1}^{1}\frac{x}{\sqrt{1-x^2}}P^m_n(x)P^m_l(x)dx\right.$$
$$+2\int_{-1}^{1}\sqrt{1-x^2}P_l^{-m}(x)\frac{\partial P^m_{l'}(x)}{\partial x}dx\cdot\int_{-1}^{1}\sqrt{1-x^2}P^m_n(x)P^m_l(x)dx-\int_{-1}^{1}xP_l^{-m+1}(x)\frac{\partial P^m_{l'}(x)}{\partial x}dx\cdot\int_{-1}^{1}xP^m_n(x)P^{m-1}_l(x)dx$$
$$\left.-\int_{-1}^{1}xP_l^{-m-1}(x)\frac{\partial P^m_{l'}(x)}{\partial x}dx\cdot\int_{-1}^{1}xP^m_n(x)P^{m+1}_l(x)dx\right] \quad (23)$$

$$\xi^{c\theta_{nm}}_{l'm'} = \frac{\pi m\delta_{m,m'}}{k\eta}\alpha a(n,m)b(l',m)(-1)^m\sum_{l=0}^{\infty}(-j)^{l-l'}\frac{(2l+1)}{2}j_l(ka)\left[\frac{-2}{ka}\int_{-1}^{1}P_l^{-m}(x)\frac{\partial P^m_{l'}(x)}{\partial x}dx\cdot\int_{-1}^{1}\frac{x}{\sqrt{1-x^2}}P^m_n(x)P^m_l(x)dx\right.$$
$$-2j\int_{-1}^{1}P_l^{-m}(x)P^m_{l'}(x)dx\cdot\int_{-1}^{1}\sqrt{1-x^2}P^m_n(x)P^m_l(x)dx+j\int_{-1}^{1}\frac{x}{\sqrt{1-x^2}}P_l^{-m+1}(x)P^m_{l'}(x)dx\cdot\int_{-1}^{1}xP^m_n(x)P^{m-1}_l(x)dx+j$$
$$\left.\int_{-1}^{1}\frac{x}{\sqrt{1-x^2}}P_l^{-m-1}(x)P^m_{l'}(x)dx\cdot\int_{-1}^{1}xP^m_n(x)P^{m+1}_l(x)dx\right]. \quad (24)$$

Table 1 Relation for the parity between n and l'.

		current along θ'		current along ϕ'	
		n: odd	n: even	n: odd	n: even
TM(ξ) degree l'	odd	-	○	○	-
	even	○	-	-	○
TE(ζ) degree l'	odd	○	-	-	○
	even	-	○	○	-

sidering the parity of the integrant for the expansion coefficient. Where the integrant is an odd function, the value of integration becomes null. It should be noted that the parity of the associated Legendre function is determined by $l + m$ as follows:

$$P^m_l(-x) = (-1)^{l+m}P^m_l(x). \quad (25)$$

2.3 Combination of Currents for Radiating Unique Eigenmode

The matrix that relates the expansion coefficients for the $(n,m)^{\text{th}}$ current and $(l',m')^{\text{th}}$ radiated field has been obtained with (21)–(24). In addition, as m' is identical to m, the coefficient for the l'^{th} field is related with that for the n^{th} current by a matrix for each m. The relation is under the constraint of the parity shown in Table 1. For example, where n for the current along θ' is odd, even-degree TM waves and odd-degree TE waves are radiated. Whereas the expansion coefficients are different, fields of the identical degrees are radiated by even-degree currents along ϕ', as shown in Table 1. Thus, even-degree TM eigenmodes and odd-degree TE eigenmodes can be synthesized by properly combining the currents along θ' and ϕ'.

Here, let a m^{th}-order desired electric field be $\boldsymbol{E}_{\text{d}}(m)$. It can also be expanded by the eigenmodes only for the m^{th} order, as follows:

$$\mathbf{Ed}(m) = \sum_{l'=1}^{\infty}\left\{\beta^{TM}_{l'}(m)\mathbf{E}^{TM}_{l'm} + \beta^{TE}_{l'}(m)\mathbf{E}^{TE}_{l'm}\right\}. \quad (26)$$

This field can be radiated by the currents as follows, where the variables are renamed simply as shown in (28):

$$\mathbf{Ed}(m) = \sum_{n=0}^{\infty}\sum_{l'=1}^{\infty}\left\{\left(c\phi_n(m)\xi\phi_{l'n}(m) + c\theta_n(m)\xi\theta_{l'n}(m)\right)\mathbf{E}^{TM}_{l'm}\right.$$
$$\left.+\left(c\phi_n(m)\zeta\phi_{l'n}(m) + c\theta_n(m)\zeta\theta_{l'n}(m)\right)\mathbf{E}^{TE}_{l'm}\right\} \quad (27)$$

$$\left.\begin{array}{ll} c\theta_n(m) \equiv c\theta_{nm} & c\phi_n(m) \equiv c\phi_{nm} \\ \xi\theta_{l'n}(m) \equiv \xi^{c\phi_{nm}}_{l'm} & \xi\phi_{l'n}(m) \equiv \xi^{c\phi_{nm}}_{l'm} \\ \zeta\theta_{l'n}(m) \equiv \zeta^{c\phi_{nm}}_{l'm} & \zeta\phi_{l'n}(m) \equiv \zeta^{c\phi_{nm}}_{l'm}. \end{array}\right\} \quad (28)$$

By comparing the coefficients for the eigenmodes, the following equations are obtained.

$$\beta^{TM}_{l'}(m) = \sum_{n=0}^{\infty}\left\{c\theta_n(m)\xi\theta_{l'n}(m) + c\phi_n(m)\xi\phi_{l'n}(m)\right\} \quad (29)$$

$$\boldsymbol{\beta} \equiv \begin{bmatrix} \beta^{TE}_{l'_1}(m) \\ \vdots \\ \beta^{TE}_{l'_1+2N-2}(m) \\ \beta^{TM}_{l'_2}(m) \\ \vdots \\ \beta^{TM}_{l'_2+2N-2}(m) \\ \beta^{TE}_{l'_1+2N}(m) \\ \vdots \\ \beta^{TM}_{l'_2+2N}(m) \\ \vdots \end{bmatrix} = \begin{bmatrix} \zeta\theta_{l'_1,n_1}(m) & \cdots & \zeta\theta_{l'_1,n_1+2N-2}(m) & \zeta\phi_{l'_1,n_2}(m) & \vdots & \zeta\phi_{l'_1,n_2+2N-2}(m) \\ \vdots & \ddots & \vdots & \vdots & \ddots & \vdots \\ \zeta\theta_{l'_1+2N-2,n_1}(m) & \cdots & \zeta\theta_{l'_1+2N-2,n_1+2N-2}(m) & \zeta\phi_{l'_1+2N-2,n_2}(m) & \cdots & \zeta\phi_{l'_1+2N-2,n_2+2N-2}(m) \\ \xi\theta_{l'_2,n_1}(m) & \cdots & \xi\theta_{l'_2,n_1+2N-2}(m) & \xi\phi_{l'_2,n_2}(m) & \cdots & \xi\phi_{l'_2,n_2+2N-2}(m) \\ \vdots & \ddots & \vdots & \vdots & \ddots & \vdots \\ \xi\theta_{l'_2+2N-2,n_1}(m) & \cdots & \xi\theta_{l'_2+2N-2,n_1+2N-2}(m) & \xi\phi_{l'_2+2N-2,n_2}(m) & \cdots & \xi\phi_{l'_2+2N-2,n_2+2N-2}(m) \\ \zeta\theta_{l'_1+2N,n_1}(m) & \cdots & \zeta\theta_{l'_1+2N,n_1+2N-2}(m) & \zeta\phi_{l'_1+2N,n_2}(m) & \cdots & \zeta\phi_{l'_1+2N,n_2+2N-2}(m) \\ \vdots & \vdots & \vdots & \vdots & \ddots & \vdots \\ \xi\theta_{l'_2+2N,n_1}(m) & \cdots & \xi\theta_{l'_2+2N,n_1+2N-2}(m) & \xi\phi_{l'_2+2N,n_2}(m) & \cdots & \xi\phi_{l'_2+2N,n_2+2N-2}(m) \\ \vdots & \ddots & \vdots & \vdots & \ddots & \vdots \end{bmatrix} \begin{bmatrix} c\theta_{n_1}(m) \\ \vdots \\ c\theta_{n_1+2N-2}(m) \\ c\phi_{n_2}(m) \\ \vdots \\ c\phi_{n_2+2N-2}(m) \end{bmatrix} \equiv A\mathbf{c} \tag{31}$$

$$\left.\begin{aligned} &n_1 = m, n_2 = m+1, l'_1 = m, l'_2 = m+1 \quad if \;\; m\text{: } odd \\ &n_1 = m+1, n_2 = m, l'_1 = m+1, l'_2 = m \quad if \;\; m\text{: } even. \end{aligned}\right\} \tag{32}$$

$$\beta^{TE}_{l'}(m) = \sum_{n=0}^{\infty} \{c\theta_n(m)\zeta\theta_{l'n}(m) + c\phi_n(m)\zeta\phi_{l'n}(m)\}. \tag{30}$$

Where N kinds of degrees n are used for both the currents along θ' and ϕ', the equations are expressed with a matrix, as shown in (31) and (32). The constraint shown in Table 1 is explicitly included in (32). Where n is less than $|m|$, the value of the associated Legendre function is null.

Here, we assume doubtfully that higher-degree modes can be neglected so that N kinds of TM waves and N kinds of TE waves may be dominant. Validity for the assumption is quantitatively checked by numerical calculations in Sect. 3.1.

With the assumption, the relation can be approximated, as shown in (33), where the reduced matrix $A^r(m)$ and the reduced field vector $\boldsymbol{\beta}^r_i$ $(i = 1, 2, \ldots, 2\mathrm{N})$ are defined by a $2N \times 2N$ matrix and a $2N$-element column vector, respectively.

$$B^r(m) = A^r(m)C(m) \tag{33}$$

$$\left.\begin{aligned} &B^r(m) \equiv (\boldsymbol{\beta}^r_1(m), \boldsymbol{\beta}^r_2(m), \cdots, \boldsymbol{\beta}^r_{2N}(m)) \\ &C(m) \equiv (\mathbf{c}_1(m), \mathbf{c}_2(m), \cdots, \mathbf{c}_{2N}(m)). \end{aligned}\right\} \tag{34}$$

Thus, the matrix $C(m)$, consisting of the current expansion coefficients, can be found in the closed form with the matrices of $[A^r(m)]^{-1}$ and $B^r(m)$ for the desired field, as follows:

$$C(m) = [A^r(m)]^{-1}B^r(m). \tag{35}$$

For the unique mode, $\boldsymbol{\beta}^r_i$ is a unit vector, and $2N$ kinds of the current expansion coefficients to synthesize the unique mode are found by the column vector elements of $[A^r(m)]^{-1}$. Thus, $2N$ kinds of eigenmodes are synthesized by $2N$ kinds of currents. In addition, by substituting the obtained $C(m)$ into (36), the exact coefficients of the fields are obtained as follows, where $\boldsymbol{\beta}_i$ is an infinite element column vector:

$$B(m) = A(m)C(m) \tag{36}$$

$$B(m) = (\boldsymbol{\beta}_1(m), \boldsymbol{\beta}_2(m), \cdots, \boldsymbol{\beta}_{2N}(m)). \tag{37}$$

For the currents to synthesize the unique modes, the matrix $B(m)$ consists of a $2N \times 2N$ unit matrix $U_{2N,2N}$ and an $\infty \times 2N$ matrix $H(m)$ that explains the expansion coefficients for undesired higher modes, as follows:

$$B(m) = \begin{bmatrix} U_{2N,2N} \\ H(m) \end{bmatrix}. \tag{38}$$

In other words, whereas a unique mode is synthesized for the $2N$ kinds of TM and TE eigenmodes, some amount of undesired higher modes is also generated. The amount is quantitatively estimated with $H(m)$.

Thus, the unique modes for even-degree TM eigenmodes and odd-degree TE eigenmodes have been synthesized by the currents $\boldsymbol{c}_i(m)$ $(i = 1, 2, \ldots, 2N)$, at least approximately. The remaining eigenmodes can also be synthesized by the currents along θ' and ϕ' with the remaining parity.

3. Numerical Calculation for Relation of Current and Radiated far Field

With the analytical formulas, numerical calculation was carried out. After checking the validity of the obtained formulas, features of the radiated fields are numerically looked into. Finally, combinations of current distributions to synthesize eigenmodes are investigated.

3.1 Estimation of Consistency for Obtained Formulas

The fields radiated by the currents along θ' and ϕ' were given by the integration shown in (4)–(6). The integration was analytically carried out, and identical fields were expressed by (18), (19) and (21)–(24). Thus, to estimate the consistency for the obtained formulas [32], the identical fields obtained in two ways were compared numerically

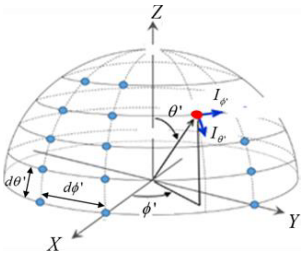

Fig. 2 Configuration for half of the analyzed discreet array.

with Mathematica^{TM}. For one of the two ways, with mode expansion, the sum for (18) and (19) was carried out up to l' of the 20$^{\text{th}}$ degree. In addition, as the continuous current distribution used for these two ways is not practical, the field generated by a discreet array was compared as a third way.

The fields were estimated both for the current along θ' and ϕ', where the degree and order were n of 2 and m of 1. The value of ka was 9. For the discreet array, infinitesimal radiating elements were located on the sphere at intervals of 10 degrees both for θ' and ϕ' directions as shown in Fig. 2, where only half of the array is depicted. The elements on the Z axis are not located. The observation points were at intervals of 5 degrees for both the θ' and ϕ' directions.

Figure 3 shows the magnitudes of the electric field estimated in the three ways. As the magnitudes were independent of ϕ for all of the estimated fields, they are shown only along θ. Considering that the three kinds of fields are identical, the formulas for the eigenmode expansion coefficients are considered to be accurate enough. In addition, the fields can be realized with the discreet array.

The phase dependence on θ and ϕ was also identical for the three ways, and was uniform and exp($j\phi$), respectively, as expected from (14) and (15).

3.2 Features of Expansion Coefficients for Radiated Fields

The relation between the expansion coefficients for the currents and the radiated fields depends on ka as well as their degrees and orders, as shown in (21)–(24). Thus, the effect of ka on the expansion coefficients was numerically estimated. For example, expansion coefficients of the fields radiated by the current along ϕ' are shown in Fig. 4, where the degree and order for the current are n of 2 and m of 1.

Whereas the order of m' is limited to being 1, there exist fields for infinite kinds of degrees of l' for both the TM and TE waves. As n is even for the current along ϕ', degrees for the TM waves are limited to being even, and those for TE waves are odd, as expected from Table 1. The magnitude increases with ka, and reaches a local maximum around l' of ka. Then, the magnitude repeatedly moves up and down. This implies that where ka is considerably smaller than l', modes for the degrees larger than l' are suppressed. In addition, to make the l'^{th}-degree mode dominant, the value of ka should not only be larger than l' but also be properly adjusted for the expansion coefficient to be around a local maximum. The relative magnitude depends also on

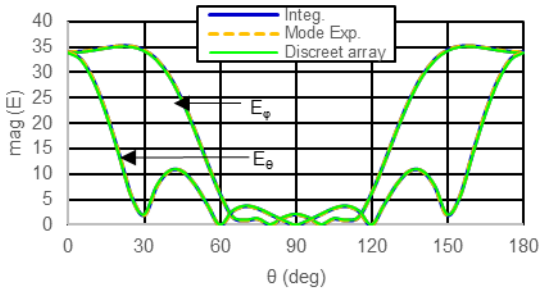

(a) Electric field radiated by current along θ'

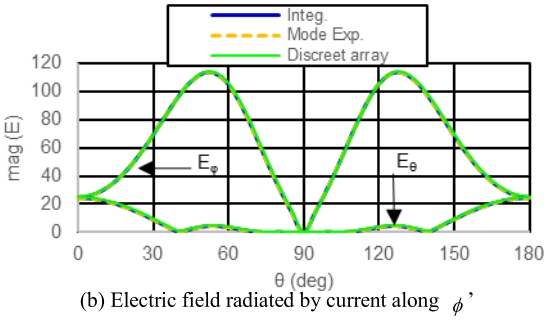

(b) Electric field radiated by current along ϕ'

Fig. 3 Comparison of the electric fields estimated in three ways. Degree and order of current: n=2, m=1.

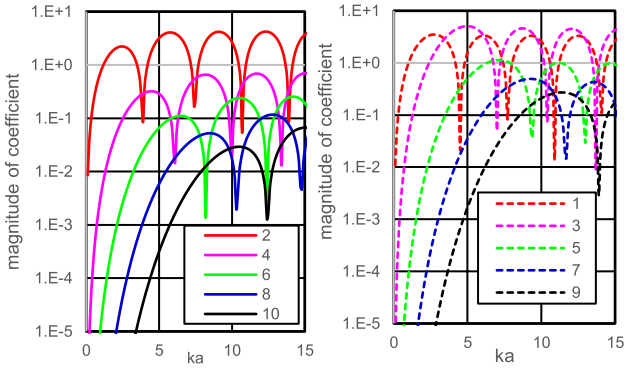

(a) TM wave (b) TE wave

Fig. 4 Magnitude of expansion coefficients for $(l', 1)^{\text{th}}$ order fields. Order of stimulated current along ϕ': n=2, m=1. The numbers in the legend denote degrees of l' for the fields.

the relation between the degrees of n and l'. The smaller the absolute value of difference for n and l', the larger the expansion coefficient becomes. In this case, the 2$^{\text{nd}}$-degree mode is dominant for the TM waves, because l' is identical to n. On the other hand, for the TE waves, as the 2$^{\text{nd}}$-degree mode is forbidden, as shown in Table 1, 1$^{\text{st}}$- and 3$^{\text{rd}}$-degree modes become dominant, where the magnitude of the upper mode is slightly larger than that of the lower one, as shown in Fig. 4(b). This implies that for an n^{th}-degree current, an $(n+1)^{\text{th}}$-degree field can be dominantly radiated, according to the condition shown in Table 1. Whereas higher modes for an l' larger than n were assumed to be neglected in Sect. 2.3, the assumption would be more appropriate to be changed so that those for l' larger than n + 1 could be neglected.

Table 2 Combination of current to generate eigenmodes, shown in (34).

	c_1	c_2	c_3	c_4	c_5	c_6
$C\theta_{11}$	-0.0493j	0.0018i	0.0010i	0.0205i	-0.0068i	-0.0063i
$C\theta_{31}$	-0.0109j	0.0115j	0.0044j	-0.0185j	-0.0479j	-0.0278j
$C\theta_{51}$	-0.0043j	0.0032j	0.0158j	-0.0046j	0.0333j	-0.1003j
$C\phi_{21}$	0.0284	0.0148	0.005404	0.0234	-0.00915	-0.0125
$C\phi_{41}$	0.0108	-0.01442	0.030337	0.0090	-0.03505	-0.0370
$C\phi_{61}$	0.0128	-0.0096	-0.0469	0.0109	-0.0330	-0.1191

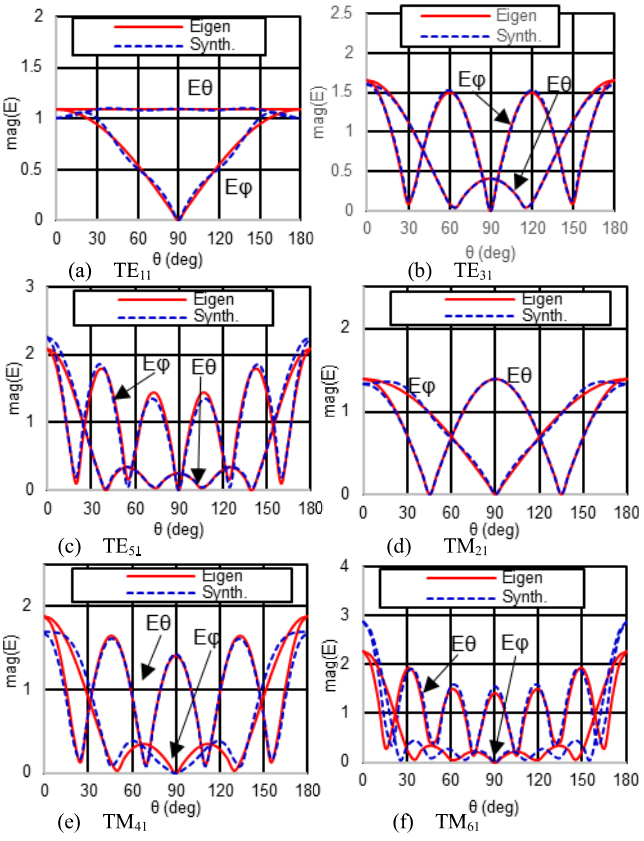

Fig. 5 Comparison of synthesized and eigenmode electric fields.

3.3 Synthesis of Unique Eigenmode by Properly Combined Current Distributions

The combination of current distributions was numerically estimated to synthesize unique eigenmodes according to the procedure shown in Sect. 2.3. Six kinds of current distributions, $c\theta_{11}/c\theta_{31}/c\theta_{51}/c\phi_{21}/c\phi_{41}/c\phi_{61}$, were utilized to synthesize six kinds of targeted unique eigenmodes, $TM_{21}/TM_{41}/TM_{61}/TE_{11}/TM_{31}/TM_{51}$, so that the currents may radiate the identical eigenmodes with fairly large expansion coefficients. The value of ka was 5. Table 2 shows the calculated combination of current, $C(m)$ shown in (35), to synthesize the eigenmodes.

Synthesized electric far fields, estimated with the combination of the currents and (27), were compared with those of the targeted eigenmodes as shown in Fig. 5. The fields agree fairly well, but the error is rather large for TM_{61} especially around θ of 0 and 180 degrees.

Table 3 Relative magnitude of higher modes expressed by $B(m)$.

	c_1	c_2	c_3	c_4	c_5	c_6
TE11	1.0000	0.0000	0.0000	0.0000	0.0000	0.0000
TE31	0.0000	1.0000	0.0000	0.0000	0.0000	0.0000
TE51	0.0000	0.0000	1.0000	0.0000	0.0000	0.0000
TM21	0.0000	0.0000	0.0000	1.0000	0.0000	0.0000
TM41	0.0000	0.0000	0.0000	0.0000	1.0000	0.0000
TM61	0.0000	0.0000	0.0000	0.0000	0.0000	1.0000
TE71	0.0336	-0.0232	-0.0769	0.0291	-0.0878	-0.3173
TE91	0.0011	-0.0008	-0.0016	0.0011	-0.0020	-0.0091
TM81	0.0000	0.0000	0.0000	-0.0003	0.0042	0.0548
TM10,1	0.0000	0.0000	0.0000	0.0000	0.0003	0.0026

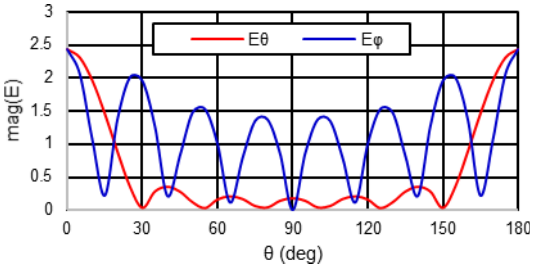

Fig. 6 Electric field for TE_{71}.

For the MIMO communication, the error is quite important, because it is closely related with the signal to interference ratio [18], [19]. Thus, to clarify the reason, the effect of undesired higher-degree modes was quantitatively analyzed with matrix $B(m)$, shown in (36). As undesired higher modes of TE_{71}, TE_{91}, TM_{81}, $TM_{10,1}$ are also radiated by the currents, their magnitudes were estimated, as shown in Table 3. Only among the targeted modes did each current distribution realize a unique mode. However, they also generate some amount of the higher modes. The magnitude of TE_{71} is much larger than those of the other higher modes, because TE_{71} is one of the dominant modes radiated by $c\phi_{61}$, as explained in Sect. 3.2. The magnitude for $\boldsymbol{c}_6$ is as large as 0.3173, which corresponds to −10.0 dB for the radiated power compared with that of the targeted TM_{61}. Thus, the error shown in Fig. 5 is considered to be explained by the field of TM_{71} shown in Fig. 6. As the magnitude of TM_{71} is large around θ of 0 and 180 degrees, the error of TM_{61} shown in Fig. 5(f) is large around the region.

As for the targeted five kinds of eigenmodes except TM_{61}, the error becomes less than 0.0878 (−21.3 dB). Thus, if additional kinds of current distributions are used for the six eigenmodes, the error would be remarkably reduced. Thus, additional current modes $c\theta_{71}$ and $c\phi_{81}$ were included. In this case, TE_{71} and TM_{81} are fully suppressed. Calculated matrix $H(m)$, shown in (38), is shown in Table 4. Where only combinations of current distributions, $\boldsymbol{c}_1$~$\boldsymbol{c}_3$ and $\boldsymbol{c}_5$~$\boldsymbol{c}_7$, are used, the targeted six modes become dominant. On the other hand, the error is reduced less than −37.2 dB. The maximum error is reduced by more than 27 dB compared with that shown in Table 3.

With the obtained results, the upper bound in the num-

Table 4 Relative magnitude (dB) of higher modes estimated with $H(m)$.

	c_1	c_2	c_3	c_4	c_5	c_6	c_7	c_8
TE91	-52.37	-55.89	-46.29	-27.46	-53.81	-44.99	-37.26	-15.56
TE11,1	-86.23	-90.10	-81.37	-64.91	-87.61	-78.79	-71.05	-49.35
TM10,2	-266.03	-281.99	-288.98	-282.18	-98.57	-78.04	-61.43	-29.99
TM10,4	-293.40	-282.62	-290.35	-284.92	-124.84	-104.71	-89.00	-59.97

ber of the modes might be roughly discussed. Let the following modes be the targeted dominant ones.

$$-l \le m' \le l', \quad 1 \le l' \le L, \quad L \gg 1 \tag{39}$$

The number of the eigenmodes (N) is about $2L^2$ as shown in (40), where there are TM and TE waves for each $(l', m')^{\text{th}}$ mode.

$$N = 2L(L+2) \approx 2L^2 \tag{40}$$

To realize $(l', m')^{\text{th}}$ mode dominant, two conditions are required, as shown in Sect. 3.2. First of all, the current distribution shown in (1) and (2) should satisfy the following condition.

$$n \approx l'm = m' \tag{41}$$

To realize every m, the number of the array elements along ϕ must be more than $2L+1$ according to the sampling theorem. Similarly, the number of the array elements along θ is considered to be more than L, possibly because the associated Legendre function is similar to the trigonometric function. Thus, the number of the required elements is similar to that of the eigenmodes.

Secondly, ka should be larger than n or l'. For the minimum radius of L/k to realize all eigenmodes, the spacing along θ between the adjacent elements is about a half-wavelength. However, the spacing along ϕ is rather narrower especially around the north and south pole. Thus, even where miniature elements are allocated, large mutual impedance effect would result. On the other hand, the effect would be reduced for a larger spherical radius, but more kinds of the current distributions should be utilized to suppress undesired higher modes.

4. Conclusion

Unique spatial eigenmodes for the spherical coordinate system were shown to be successfully synthesized by properly allocated combinations of current distributions along θ' and ϕ' on a spherical conformal array. The allocation ratios were analytically found in a closed form with a matrix that relates the expansion coefficients of the current to its radiated field. The coefficients were obtained by general Fourier expansion of the current and the mode expansion of the fields. The validity of the obtained formulas was numerically confirmed, and important effects of the sphere radius and the degrees and orders of the current on the radiated fields were numerically explained. The formulas were used to design current distributions that synthesize six unique eigenmodes. The accuracy was quantitatively investigated, and the accuracy was shown to be improved by more than 27 dB with the two additional kinds of current distributions.

Acknowledgments

This research and development work were partly supported by KAKENHI 19K04387.

References

[1] L.J. Chu, "Physical limitations of omni-directional antennas," J. Appl. Phys., vol.19, pp.1163–1175, 1948.
[2] R.F. Harrington, Time-Harmonic Electromagnetic Fields, pp.264–316, U.S., IEEE Press, 2001.
[3] J.D. Jackson, Classical Electrodynamics 3rd ed., pp.407–448, John Wiley & Sons, U.S., 1999.
[4] A. Saitou, K. Aoki, K. Honjo, and K. Watanabe, "Design consideration on the minimum size of broadband antennas for UWB applications," IEEE Trans. Microwave Theory Techn., vol.56, no.1, pp.15–21, Jan. 2008.
[5] S. Ito, N. Inagaki, and T. Sekiguchi, "An investigation of the array of circular-loop antennas," IEEE Trans. Antennas Propag., vol.AP-19, no.4, pp.469–476, July 1971.
[6] S. Krishnan, L. Li, and M. Leong, "Entire-domain MoM analysis of an array of arbitrarily oriented circular loop antennas: A general formulation," IEEE Trans, Antennas Propag., vol.53, no.9, pp.2961–2968, Sept. 2005.
[7] S.M.A. Hamed, "Exact field expression for circular loop antennas using spherical functions expansion," IEEE Trans. Antennas Propag., vol.61, no.6, pp.2956–2963, June 2013.
[8] R.J. Mailloux, Phased Array Antenna, 3rd ed., pp.197–234, Artech Hous, U.S., 2018.
[9] L. Josefsson, P. Persson, Conformal Array Antenna Theory and Design, pp.23–34, IEEE Press, U.S., 2006.
[10] R. Goossens, I. Bogaert, and H. Rogier, "Phase-mode processing for spherical antenna arrays with a finite number of antenna elements and including mutual coupling," IEEE Trans. Antennas Propag., vol.57, no.12, pp.3783–3790, Dec. 2009.
[11] T.D. Abhayapala and A. Gupta, "Spherical harmonic analysis of wavefields using multiple circular sensor arrays," IEEE Trans. Audio, Speech, Language Process., vol.18, no.6, pp.1655–1666, Aug. 2010.
[12] L. Allen, M.W. Beijersbergen, R.J.C. Spreeuw, and J.P. Woerdman, "Orbital angular momentum of light and the transformation of Laguerre-Gaussian laser modes," Phys. Rev. A., vol.45, no.11, pp.8185–8189, June 1992.
[13] S.M. Mohammadi, L.K.S. Daldorff, J.E.S. Bergman, R.L. Karlsson, B. Thidé, K. Forozesh, T.D. Carozzi, and B. Isham, "Orbital angular momentum in radio — A system study," IEEE Trans. Antennas Propag., vol.58, no.2, pp.565–572, Feb. 2010.
[14] J. Wang, J.-Y. Yang, I.M. Fazal, N. Ahmed, Y. Yan, H. Huang, Y. Ren, Y. Yue, S. Dolinar, M. Tur, and A.E. Willner, "Terabit free-space data transmission employing orbital angular momentum multiplexing," Nature Photon., vol.6, pp.488–496, July 2012.
[15] F. Tamburini, E. Mari, A. Sponselli, B. Thid é, A. Bianchini, and F. Romanato, "Encoding many channels on the same frequency through radio vorticity: First experimental test," New J. Phys., vol.14, pp.1–17, March 2012.
[16] Q. Bai, A. Tennant, and B. Allen, "Experimental circular phased array for generating OAM radio beams," Elec. Lett., vol.50, no.20, pp.1414–1415, 2014.
[17] D. Lee, H. Sasaki, H. Fukumoto, K. Hiraga, and T. Nakagawa, "Orbital angular momentum multiplexing: An enabler of a new era of wireless communications," IEICE Trans. Commun., vol.E100-B, no.7, pp.1044–1063, July 2017.

[18] A. Saitou, R. Ishikawa, and K. Honjo, "4-value multiplexing orbital-angular-momentum communication scheme using loop-antenna arrays," APMC, Dec. 2016.
[19] H. Otsuka, Y. Yamagishi, A. Saitou, H. Suzuki, R. Ishikawa, and K. Honjo, "High performance OAM communication exploiting port-azimuth effect of loop antennas," IEICE Trans. Commun., vol.E102-B, no.12, pp.2267–2275, Dec. 2019.
[20] R. Yamagishi, H. Otuka, A. Saitou, R. Ishikawa, and K. Honjo, "Improvement of mode uniqueness for OAM communication using a loop array with reflector plane," 2017 Asia Pacific Microwave Conference, Nov. 2017.
[21] M. Arai, M. Iwabuchi, K. Sakaguchi, and K. Araki, "Optimal design method of MIMO antenna directivities and corresponding current distributions by using spherical mode expansion," IEICE Trans. Commun., vol.E100-B, no.10, pp.1891–1903, Oct. 2017.
[22] Y. Kang and D.M. Pozar, "Correction of error in reduced sidelobe synthesis due to mutual coupling," IEEE Trans. Antennas Propag., vol.AP-33, no.9, pp.1025–1028, Sept. 1985.
[23] Z. Huang, C.A. Balanis, and C.R. Birtcher, "Mutual coupling compensation in UCAs: Simulations and experiment," IEEE Trans. Antennas Propag., vol.54, no.11, pp.3082–3086, Nov. 2006.
[24] R. Goossens, I. Bogaert, and H. Rogier, "Phase-mode processing for spherical antenna arrays with a finite number of antenna elements and including mutual coupling," IEEE Trans. Antennas Propag., vol.57, no.12, pp.3783–3790, Dec. 2009.
[25] D.L. Sengupta, T.M. Smith, and R.W. Larson, "Radiation characteristics of a Spherical array of circularly polarized elements," IEEE Trans. Antennas Propag., vol.AP-16, no.1, pp.2–7, Jan. 1968.
[26] B. Tomasic, J. Turtle, and S. Liu, "Spherical arrays — Design considerations," Int. Conf. on Applied Electromagnetics and Communications, 2005.
[27] B.P. Kumar, C. Kumar, V.S. Kumar, and V.V. Srinivasan, "Active spherical phased array design for satellite payload data transmission," IEEE Trans. Antennas Wireless Propag., vol.63, no.11, pp.4783–4790, Nov. 2015.
[28] B.P. Kumar, C. Kumar, V.S. Kumar, and V.V. Srinivasan, "Optimal radiation pattern of the element for a spherical phased array with hemispherical scan capability," IEEE Antennas Wireless Propag. Lett., vol.16, pp.2780–2782, 2017.
[29] J. Zhang, P. Liu, Z. Zhuang, J. Wei, X. Liu, H. Wang, and L. Li, "Design of a spherical conformal phased array antenna based on the truncated icosahedron," IEEE Radar Conference, 2020.
[30] F.W.J. Olver, D.W. Lozier, R.F. Boisvert, and C.W. Clark, NIST Handbook of Mathematical Functions, pp.351–382, 2010.
[31] C.A. Balanis, Antenna Theory 3rd ed., pp.133–144, J. Wiley & Sons, U.S., 1999.
[32] Y. Chen and T. Simpson, "Radiation pattern analysis of arbitrary wire antenna using spherical mode expansions with vector coefficients," IEEE Trans. Antennas Propag., vol.39, no.12, pp.1716–1721, Dec. 1991.

Akira Saitou received his B.E. and M.E. degrees in applied physics from the University of Tokyo in 1975 and 1977, respectively, and his D.E. degree from the University of Electro-Communications in 2008. From 1977 to 2002, he was employed at NEC Corporation to develop GaAs FETs and MMICs for microwave and millimeter-wave communication. From 2002–2009, he worked for YKC Corporation to develop microwave circuits and antennas. In 2009, he joined the University of Electro-Communications as a guest professor.

Ryo Ishikawa received the B.E., M.E., and D.E. degrees in electronic engineering from Tohoku University, Sendai, Japan, in 1996, 1998, and 2001, respectively. In 2001, he joined the Research Institute of Electrical Communication, Tohoku University. In 2003, he joined the University of Electro-Communications, Tokyo, Japan. His research interest is the development of microwave compound semiconductor devices and related techniques. Dr. Ishikawa is a member of the Japan Society of Applied Physics. He was the recipient of the 1999 Young Scientist Award for the Presentation of an Excellent Paper of the Tohoku Chapter, Japan Society of Applied Physics.

Kazuhiko Honjo received the B.E. degree from the University of Electro-Communications in 1974, and the M.E. and D.E. degrees in electronic engineering from the Tokyo Institute of Technology in 1976 and 1983, respectively. From 1976 to 2001, he worked for NEC Corporation, Kawasaki, Japan. In 2001, he joined the University of Electro-Communications as a professor in the Information and Communication Engineering Department. He has been involved in research and development of high-power/broadband/low-distortion microwave amplifiers, MMICs, HBT device and processing technology, miniature broadband microwave antennas and FDTD electro-magnetic wave and device coanalysis. Prof. Honjo received both the 1983 Microwave Prize and the 1988 Microwave Prize granted by the IEEE Microwave Theory and Techniques Society. He also received the 1980 Young Engineer Award, and the 1999 Electronics Award both presented by the Institute of Electrical, Information and Communication Engineers (IEICE), Japan. He is Fellow of IEEE.